DAPI staining and DNA content estimation of uncultivable microbial eukaryotes' nuclei (Arcellinida and Ciliates)

Ketty Munyenyembe^{a,*}, Caitlin Timmons^{a,*}, Agnes KM Weiner^a, Laura A Katz^{a,b,†}, Ying Yan^{a,#,†}

^a Smith College, Department of Biological Sciences, Northampton, Massachusetts, USA

^b University of Massachusetts Amherst, Program in Organismic and Evolutionary Biology, Amherst, Massachusetts, USA

^{*} Both authors contributed equally to this work

[#] Current address: Laboratory of Protozoology, Institute of Evolution and Marine Biodiversity, Ocean University of China, Qingdao, China

[†] Corresponding authors. E-mail: <u>lkatz@smith.edu</u>, <u>yingyan@ouc.edu.cn</u>

Abstract

Though acting as a major component of eukaryotic biodiversity, many microbial eukaryotes

remain poorly studied, including the focus of the present work, testate amoebae of the order

Arcellinida (Amoebozoa) and non-model lineages of ciliates (Alveolata). In particular, knowledge

of their genome structures and changes in genome content over their often-complex life cycles

remains enigmatic. However, the limited available knowledge suggests that microbial

eukaryotes have the potential to challenge our textbook views on eukaryotic genomes and

genome evolution. In this study, we developed protocols for DAPI (4',6-diamidino-2-

phenylindole) staining of Arcellinida nuclei and adapted protocols for ciliates. In addition, image

analysis software was used to estimate the DNA content in the nuclei of Arcellinida and ciliates

and to compare them to measurements of well-known model organisms. The results

demonstrate that the methods we have developed for nuclear staining in these lineages are

effective and can be easily applied to other microbial eukaryotic groups by adjusting certain

stages in the protocols.

Keywords: DAPI staining; DNA content; ciliates; Arcellinida; protists; nucleus

Introduction

The bulk of all biodiversity, and by extent eukaryotic diversity, is microbial. Microbial eukaryotes (i.e. protists) exhibit diverse and dynamic genome structures. Their genomes span a large range of sizes, from little over 2 Mb in some microsporidians to over 670,000 Mb in *Amoeba dubia* (reviewed in: McGrath and Katz, 2004). They also exhibit a number of unusual features, such as nuclear dualism (e.g. McGrath and Katz, 2004; Prescott, 1994), extensive genome fragmentation (e.g. Huang and Katz, 2014; Swart et al., 2013), and genome increase/reduction (Parfrey et al., 2008). Despite their unusual characteristics, studies of nuclear structures and genome sizes in microbial eukaryotes remain limited (e.g. Grattepanche et al., 2018). Given their diversity, characterizing the nuclear architectures and genome structures of microbial eukaryotes furthers our understanding of eukaryotic biodiversity and, more broadly, evolutionary principles.

Basic features such as nuclear number, structure, and estimated genome sizes are especially under-studied in testate amoebae (Arcellinida, Amoebozoa) and ciliates (Alveolata), the focal clades in this study. Testate amoebae are single-celled eukaryotes that build tests (shells) either from environmental materials or through biosynthesis (e.g. Mitchell et al., 2008; Nikolaev et al., 2005). These tests have been used traditionally as a feature of species identity. Arcellinida are mostly found in freshwater terrestrial habitats (e.g. Mitchell et al., 2008; Mitchell and Meisterfeld, 2005; Nikolaev et al., 2005) and since they are sensitive to environmental changes they are used as bioindicators for changing environmental conditions (Mieczan, 2009; Swindles et al., 2016). To date, we have only limited knowledge on Arcellinida genomes, mostly from transcriptome analyses (e.g. Lahr et al., 2019; Weiner et al., 2020) and no reference genome exists, to the best of our knowledge. Studies that have explored genomes in Amoebozoa have done so in pathogenic amoeba and slime molds (e.g. Bloomfield, 2016; Chávez-Munguía et al.,

2006; Mukherjee et al., 2009), which are likely >500 million years divergent from Arcellinida. Notably, only few studies have attempted to explore Arcellinida life cycle stages due to the fact that they are uncultivable. However, even though life cycle stages of Arcellinida are not understood in depth, Cavallini (1926) provides evidence which suggest that testate forms of Arcellinida produce naked offsprings. In addition, Volkova and Smirnov (2016) showed that if *Arcella* are removed from their tests, they are capable of generating new tests although subsequent division was not observed.

Another group of single cell eukaryotes, ciliates, has challenged the traditional views of eukaryotic nuclear structure. Ciliates are characterized by the presence of hair-like cilia and nuclear dimorphism, meaning presence of somatic macronuclei and germline micronuclei, within a single cell (e.g. Prescott, 1994). The somatic macronuclei are responsible for the majority of cellular activity, while germline micronuclei are quiescent for most of the life cycle. Within ciliates, there is a great diversity of nuclear structures. Our target organism *Loxodes* belongs to the class Karyorelictea, which is unique among ciliates in that their somatic macronuclei do not divide (Raikov, 1985). When the cell undergoes division, at least one somatic macronucleus is passed directly to the daughter cells, and germline micronuclei divide and differentiate to form new somatic macronuclei. Somatic macronuclei are believed to persist through several generations before degradation, and may experience changes in DNA content and morphology as they age (i.e. being kept for several generations; Raikov, 1985; Yan et al., 2017). Although the number and structure of nuclear groups in *Loxodes* species has been fairly well classified (Raikov, 1985; Ron and Urieli, 1977), these observations were conducted in an era before modern microscopy techniques.

Fluorescence microscopy is a powerful method that allows for detailed observations of nuclear structure in microbial eukaryotes as well as estimates of genome content and ploidy level

(Bellec et al., 2014; Maurer-Alcalá and Katz, 2016; Parfrey and Katz, 2010a; Parfrey and Katz, 2010b; Wancura et al., 2018). The method of quantifying fluorescence to estimate genome content has been used in studies of plant species (Cousin et al., 2009; Loureiro et al., 2006; Suda and Trávníček, 2006), Foraminifera (*Allogromia laticollaris*, Parfrey and Katz, 2010b), ciliate species (*Blepharisma americanum*, Wancura et al., 2018) and myxomycetes (Therrien & Collins 1976; Ritch & Therrien 1988). However, previous studies that have used these approaches to analyze nuclear structures in testate amoeba have failed despite numerous attempts to modify protocols (e.g. Burdikova et al., 2010). Therefore, according to our knowledge, a reliable method for revealing nuclear architecture in testate amoebae has not yet been described.

In this study, we investigate the nuclear structure and estimate the genome content of two genera of microbial eukaryotes: the testate amoebae *Hyalosphenia* and the ciliate *Loxodes*. Here, we describe the staining protocols for testate amoebae and ciliates that were developed and adapted for this work, respectively, following methods from Parfrey et al., (2010b) and Wancura et al., (2018). We rely on DAPI (4',6-diamidino-2-phenylindole), a standard nuclear stain but one with known limitations, notably that it preferentially binds to A-T rich chromosomal regions and thus may provide inaccurate estimates of genome content (Noirot et al., 2002). Furthermore, we use both protocols to stain organisms with known genome sizes and estimate the genome content of our organisms.

Material and Methods

Sample collection

Samples of freshwater and sediment were collected for *Loxodes* cells and *Sphagnum* moss for isolating *Hyalosphenia* species, both from Hawley bog (Hawley, MA) between June and November 2019. *Loxodes* cells were picked from the water samples using a hand pipette. The

Sphagnum moss was washed in the lab using filtered (2 µm filter) bog water and poured over a 300 µm filter to isolate testate amoeba from larger plant material. The amoeba cells were then placed in a Petri dish from which they were individually picked using a hand pipette, washed again in filtered bog water and placed into a 3.0 ml tube.

Cell fixation and DAPI staining

Loxodes cells were stained following a protocol modified from Wancura et al. (2018). Cells were placed on Superfrost slides (Fisher, Waltham, MA) in 200 µL Volvic water. They were fixed directly on the slides with a mixture of 20% Paraformaldehyde (PFA), RNAlater, and Trizol for 30 minutes, and washed 3 times for 5 minutes with 1x Phosphate-buffered saline (PBS) buffer. Fixatives and buffers were added and removed from the slide using micropipettes. Cells were then incubated in 40 µL of 0.5 % Triton-X for 25 minutes and washed again 3 times for 5 minutes with 1x PBS buffer. The slides were then incubated in a pre-hybridization mix consisting of a 1:1 ratio of Formamide and 2x saline-sodium citrate buffer (SSC) for 30 minutes at room temperature, and hybridized in a solution of Nuclease-Free Water, Formamide, and 20x SSC in a 5:4:1 ratio for 1 hour at 37 °C. Slides were washed three times with 2x SSC for 5 minutes, and incubated in DAPI (5 mg/ml, 1:1000 or 1:100 dilution; Fisher) for 5 minutes. DAPI was washed off 3 times for 2 minutes each with 1x PBS. A drop of SlowFadeGold (Invitrogen, Carlsbad, CA) was then added. The slides were sealed with a coverslip and nail polish and kept in the dark at 4 °C before being examined under a microscope.

Arcellinida cells were fixed in 400 µL of 0.2 M, pH 7.2 PHEM (PIPES-Hepes-Ethylene glycol tetraacetic acid (EGTA)-MgCl₂) buffer (Electron Microscopy Sciences Hatfield, PA United States) in a microcentrifuge tube and were incubated for 2 hours at room temperature. After 2 hours, the fixed cells were gently spun on a mini centrifuge for 30 seconds to form a pellet at the bottom of the tube and the supernatant was removed. Fixed cells were then washed twice in

400 μ L 1x PBS buffer. After the washing step, the cells were incubated for two hours in 400 μ L of 10 % Triton-X for membrane permeabilization. After the incubation period, Triton-X was removed and the cells were washed twice in 400 μ L 1x PBS. Fixed and permeabilized cells were incubated in 100 μ L DAPI (5 mg/ml, 1:100 dilution; Fisher) for 2 hours in darkness. DAPI was then washed off twice using 400 μ L 1x PBS. Stained cells were placed on a Superfrost slide (Fisher) with a drop of Slow Fade Gold (Invitrogen), covered with a cover slip and sealed with nail polish.

Both of these newly-developed fixation protocols (20% PFA for *Loxodes* vs PHEM buffer for *Hyalosphenia*) were also applied to *Saccharomyces cerevisiae* cells, *Homo sapiens* epithelial cells and *Allium cepa* root tip cells in order to understand the influence of fixation methods on staining intensity, the ratio of nuclear fluorescence to DNA content in Arcellinida and *Loxodes*, and to demonstrate that our protocols work on a variety of eukaryotic cells.

Fluorescent Imaging

Fluorescent images of all cells were collected on a Leica TCS SP5 laser-scanning confocal microscope (Leica, Mannheim, Germany) using a 63x oil immersion objective. A UV laser with an excitation wavelength of 405 nm, set to 20% intensity, was used to collect DAPI signals, and an argon laser with an excitation wavelength of 488 nm, set to 20% intensity, was used to collect differential interference contrast (DIC) images. Z-stacks of *Loxodes, A. cepa, S. cerevisiae*, and *H. sapiens* were collected at a resolution of 1024 x 1024 with an acquisition speed of 200 Hz, a line average of 4, and a step size of 0.13 µm. Z-stacks of Arcellinida were collected at a resolution of 1024 x 1024 with an acquisition speed of 200 Hz, a line average of 2, and a step size of 0.13 µm. The gain setting varied slightly across all images to adjust for variability in cell fixation and DAPI penetrance. We examined each cell's morphology and image quality in the DIC images, and only considered those that were fixed and imaged well for our

analyses of nuclear size, fluorescence, and DNA content. We counted the number of nuclei present in each cell, inspected them for the presence of nucleoli and measured the diameter of the nuclei using ImageJ software (Rasband, W.S. ImageJ. U.S National Institutes of Health, Bethesda, MD; **Table 1**).

DNA Content Estimation

In addition to nuclear number and diameter, we also measured the fluorescence intensities and nuclear volumes for *Loxodes* macronuclei, *Loxodes* micronuclei and the nuclei of *Hyalosphenia papilio*, *Hyalosphenia elegans*, *S. cerevisiae*, *H. sapiens*, and *A. cepa* (**Table 1**; **Table 2**). *Z*-stacks of nuclei were analyzed using the General Analysis 3 feature of NIS-Elements Advanced Research software (Nikon, Tokyo, Japan). The threshold setting was manually determined for each z-stack analyzed to ensure that nuclear volumes were defined accurately before measurement. For each nucleus, the volume, total fluorescence intensity (measured in K), and mean fluorescence intensity were measured (**Table 2**). *S. cerevisiae*, *H. sapiens*, and *A. cepa* nuclei were used as standards for comparison of *Loxodes* and Arcellinida measurements to assess the variability in fluorescent intensities produced by DAPI staining, as the genome content of these cells is well known.

The ratio of fluorescence to DNA content was calibrated following methods from Wancura et al. (2018). For each standard, the ratio of fluorescence to DNA content was calculated using the average measurement of nuclear fluorescence in that organism and its published genome size. The average of these three calculations was used as the final ratio by which we estimated the DNA content in *Loxodes* and *Hyalosphenia* nuclei.

Results

Protocols for fixation and DAPI staining of uncultivable microbial eukaryotes

We developed protocols to successfully stain the nuclei of two lineages of uncultivable microbial eukaryotes: the ciliate genus *Loxodes* (Ciliophora: Karyorelictea) and the testate amoeba genus *Hyalosphenia* (Tubulinea: Arcellinida). Steps for these protocols involve isolation of cells from nature, and fixation in buffers that vary between the two lineages (**Fig.1**). Protocol development required many trials as each species requires specific fixation methods. For example, *Loxodes* cells burst when spun in tubes or immersed in 'standard' fixatives such as ethanol or methanol, but we demonstrate that their nuclei can be stained following fixation in 20% PFA and membrane permeabilization in a low concentration of Triton-X. In contrast, Arcellinida cell membranes remain impermeable in many common fixative chemicals including PFA, ethanol, and methanol; instead, we found that PHEM buffer followed by membrane permeabilization using Triton X allows staining of Arcellinida nuclei. The robust methods we developed worked for visualizing nuclear number and structures in our study organisms and, in addition, we applied them to estimate nuclear volume and DNA content of Arcellinida and *Loxodes*.

As control organisms for estimates of genome size, we stained the nuclei of *Saccharomyces cerevisiae*, *Allium cepa* and *Homo sapiens* cheek cells according to both protocols: the PFA protocol developed specifically for *Loxodes* and the PHEM protocol developed specifically for *Hyalosphenia*. We observed similar fixation quality, cell morphology, and fluorescent intensity among high-quality slides of standard cells imaged according to both protocols (**Table S1**, **Fig. S2**). On cells from slides with spurious issues unrelated to the specific staining protocol, we measured artificially low nuclear fluorescent intensity (**Table S1**, **Fig. S2**). As such, we selected the cells from high-quality slides with the best morphology and image quality to use in our analyses. Therefore, for the final estimates of DNA content, we used *S. cerevisiae* cells stained according to the *Loxodes* protocol, while the chosen *A. cepa* and *H. sapiens* cells were stained according to the PHEM protocol for *Hyalosphenia*. In our analyses, we omitted *S. cerevisiae* cells generated from the PHEM protocol for *Hyalosphenia*, because the cells were so densely

arranged on the slide—as seen through DIC images—that their DAPI signal was compromised and they posed an interference to the measurements. We omitted *A. cepa* cells stained according to the PFA protocol for *Loxodes* because cells on some slides were obscured by debris, which affected DAPI penetration. *H. sapiens* cells from both protocols all came from high-quality slides and yielded similar fixation quality, cell morphology, and fluorescent signal across both protocols (**Table S1**, **Figure S2**). We chose to use *H. sapiens* cells stained according to the PHEM protocol for *Hyalosphenia* in our analyses because the positions of these cells lent themselves to more effective detection of nuclear volume with our image analysis software than some cells stained according to the PFA protocol for *Loxodes*.

Nuclear number and structures in Loxodes and Hyalosphenia

In total, we imaged and analyzed the nuclei of 29 *Loxodes* cells, 25 *Hyalosphenia* papilio cells, 3 *Hyalosphenia* elegans cells, 63 *S. cerevisiae* cells, 43 *H. sapiens* cells, and 19 *A.* cepa cells (**Table 1**). Our results show that *Loxodes* cells generally have two nuclear groups, each consisting of a spherical somatic nucleus and a germline nucleus (**Fig. 2**). Our observation of the nuclear architecture in *Loxodes* is consistent with previous studies (eg.Raikov, 1982; Raikov, 1985). The germline nucleus is smaller in size (3.5 µm in diameter on average, **Table 1**), appears to be evenly stained and has a stronger fluorescent signal, while the somatic nuclei have a greater diameter (6.6 µm on average, **Table 1**) and show a much fainter and uneven DAPI signal (**Fig. 2**). A large unstained round area (about 3.6 µm in diameter on average) is located in the center of most somatic nuclei, making them appear ring-shaped in the fluorescent images (**Fig. 2**). We suggest that this unstained area represents the nucleolus, in accordance with Raikov (1985), who noted that this area stains intensely for RNA and protein. We never observed more than one nucleolus in a single nucleus, and in five of 29 cells, a smaller nucleolus or even no obvious nucleolus was detected. However, in one of 29 cells we observed

more than four somatic nuclei and in five of 29 cells we observed more than two, and a maximum of five, germline nuclei (**Table 1**).

In both species of Hyalosphenia: *H. papilio* and *H. elegans*, we observed a single nucleus. *H. papilio* nuclei appear spherical and range from 8.0-30.8 µm (18.3 µm on average) in diameter within uninucleate cells (**Table 1**). *H. elegans* nuclei also appear spherical, however they are generally smaller than *H. papilio* nuclei, ranging from 7.3-14.3 µm (10.7 µm on average) in diameter (**Table 1**). The location of the nucleus varied in different cells: in some cells the nucleus was in the center of the cell while in other cells it was at the edge, close to the shell (**Fig. 2**), though location may be driven by fixation and cell orientation on the microscope slide. In the DIC images, nuclei are discernable in only some *H. papilio* and are easier to see in *H. elegans* (e.g. **Fig. 2**). In five of 25 *H. papilio* cells, we saw multiple nuclei ranging in size from 8.5 -17.2 µm in diameter (11.4 µm on average), with up to nine in one case (**Fig. S1, Table 1**).

Estimates of nuclear size and DNA content in target species

In the present study, we report DNA content estimates for *Hyalosphenia papilio*, both the somatic macronuclei and germline micronuclei of *Loxodes*, and the three "standards" onion, yeast and human cheek cells. The fluorescence of our three standard organisms' nuclei was consistent with their relative genome sizes, i.e., *A. cepa* has larger genomes compared to *H. sapiens* and then *S. cerevisiae* (e.g. Palazzo and Gregory, 2014). We exclude the measurements of *H. elegans* cells for this analysis, because of its small sample size. Interpolating from the standards with known genome size, we estimate that DNA content in the *Loxodes* somatic macronuclei $(3,500 \pm 1,732 \text{ Mb})$ is approximately 2.5 times higher than the DNA content in the germline micronuclei $(1,400 \pm 927 \text{ Mb})$; **Fig. 4, Table 2**). Additionally, in five of our 29 *Loxodes* cells, the measurement of one macronucleus is more than twice the

estimated DNA content of the other, which may indicate the 'age' difference between the two macronuclei. For H. papilio, we estimate a genome size of $20,900 \pm 17,759$ Mb for uninucleate cells and $11,200 \pm 8,209$ Mb for multinucleated cells, which is a very large size and surpasses even the onion genome ($15,876 \pm 4,783$ Mb; **Fig. 4, Table 2**). This result is consistent with our observations of nuclear morphology, in which the H. papilio nuclei were by far the largest in terms of diameter and volume (**Table 2, Table S2**). Multinucleated and uninucleate H. papilio cells not only differed in terms of nuclear number, but also in size and DNA content (**Fig. 4, Table 2**). Uninucleate H. papilio nuclei measured $\sim 830 \ \mu m^3$ on average and nuclei of multinucleated cells reached only half the size with $\sim 474 \ \mu m^3$ on average (**Table S2**). DNA content for uninucleate cells was ~ 21 Gb while multinucleated cells had ~ 11.2 Gb (**Table 2**).

Discussion

Methods development for nuclear staining in uncultivable microbial eukaryotes

We have successfully developed protocols for nuclear fluorescent staining in members of two distinct clades of uncultivable eukaryotic microbes, *Loxodes* (Ciliophora) and *Hyalosphenia* (Arcellinida) with the emphasize on effective fixation. PHEM buffer, which acts as fixative in *Hyalosphenia* species, has been shown to be an excellent fixative agent for marine invertebrates (Montanaro et al., 2016) and for foraminifera (Parfrey and Katz, 2010b; Weber and Pawlowski, 2013) because of its ability to permeabilize tough membranes while preserving cell morphological structures. It is also noticeable that though *Loxodes* cells can be fixed successfully in multiple solutions used for morphological studies (e.g. silver staining), such as osmium tetroxide (Finlay and Berninger, 1984), Nissenbaum's sublimate mixture (Bobyleva et al., 1980), Lugol's iodide, and mercuric chloride (Sime-Ngando et al., 1990), DAPI staining protocols that can successfully reveal nuclear structures in other ciliate groups (e.g. Bellec et al., 2014; Sun et al., 2009) cannot be directly applied to *Loxodes*. The cells burst when

incubated in common fixatives used for fluorescent microscopy work, such as ethanol and methanol (unpublished data), while Arcellinida cells are difficult to penetrate by these fixatives.

This indicates that cell membrane properties vary considerably. Therefore, potential adjustment might be required when using the present respective protocols to other related organisms.

Nuclear features and estimates of genome size in *Hyalosphenia* and *Loxodes*

Our analyses demonstrate that the majority of *Hyalosphenia* cells have one spherical nucleus, consistent with observations of other Arcellinida genera including *Phryganella acropoda* (Dumack et al., 2020) and *Difflugia* sp. (Griffin, 1972; Mazei and Warren, 2014; Volkova and Smirnov, 2016). A few *H. papilio* cells with more nuclei than expected were also observed (**Table 1; Fig. 3**). We hypothesize that the multinucleated cells may be undergoing cell division and/or may represent specific life-history stages consistent with Mignot and Raikov (1992) who suggested that meiosis occurs in cysts of *Arcella vulgaris*. Most strikingly, the multinucleated cells show smaller nuclei (avg. 11.4 μm) compared to uninucleate cells (18.3 μm; **Table 1**) indicating DNA reduction in relation with nuclear size.

Our results also suggest that *H. papilio* bears a huge genome, twice the genome size of humans (**Fig. 4, Table 2**), which is consistent with previous estimates of Amoebozoa genomes; for example, *Amoeba dubia* has the largest eukaryotic genome size known to date with an estimate of ~ 670 Gb (Friz, 1968). Also, it must be acknowledged that genome dynamics in Amoebozoa are very complex. For example, Goodkov et al., (2020) report DNA extrusion during the life cycle of *Amoeba proteus*. Similarly, the amoebozoan parasite *Entamoeba* varies in DNA content at different life stages, perhaps because of its poor control in DNA segregation (Mukherjee et al., 2009). Myxomycetes are characterized by a wide range of genome sizes and differences in ploidy even within individual strains, as extensively reviewed in Clark & Haskins (2013). We therefore hypothesize that *H. papilio* has variable ploidy levels consistent with

findings of aneuploidy in other amoebozoan lineages (Byers, 1986; Friz, 1968). Additionally, we speculate that the change in nuclear volume and DNA content between multinucleate and uninucleate *H. papilio* suggests a possible reduction in DNA during meiosis, but additional data and a more robust sample size will be required to test this possibility.

The observations on Loxodes nuclear architecture are congruent with previous work on this genus (e.g. Raikov, 1982; Raikov, 1985) as we consistently observe a minimum of two somatic macronuclei and germline micronuclei per cell. The somatic macronucleus contains only one nucleolus located in the center of the nucleus, and the micronuclear architecture is similar to other ciliate species in that DNA appears densely and uniformly distributed (Prescott, 1994). The estimate of the germline micronuclear genome in Loxodes sp. is ~1.4 Gb, which is larger than that of previously characterized ciliates species, e.g. 82.9 Mb for Paramecium tetraurelia (Oligohymenophorea: Arnaiz et al., 2012),157 Mb for Tetrahymena thermophila (Oligohymenophorea: Hamilton et al., 2016), and ~500 Mb for Oxytricha trifallax (Spirotrichea: Chen et al., 2014). It is possible that Loxodes indeed has a large and complex genome, though the AT binding preference of DAPI staining might have contributed to an overestimation of the genome size. The Loxodes genome likely has a higher AT content than the genomes of the three standard organisms used to calibrate the ratio of fluorescence units to DNA content for our staining protocol (Piovesan et al., 2019; Ricroch and Brown, 1997; Wang and Gao, 2019). Also, DAPI is known to overestimate DNA content in AT-rich genomes relative to GC-rich genomes (Button and Robertson, 2001; Wheeler et al., 2012). A previous study showed that karyorelictids, the group Loxodes belongs to, tend to have less transcripts in conserved gene families referring to smaller gene families (Yan et al., 2019). It could be assumed that the germline micronuclear genome in Loxodes is enriched with germline specific information that is not protein coding.

The macronuclear DNA content is estimated to be greater than micronuclear DNA content, consistent with previous fluorescent studies of ciliate genomes (e.g. Wancura et al., 2018). The estimate of the *Loxodes* somatic macronuclear genome size, approximately 3.5 Gb, is large compared to other ciliates. For example, the model lineages *O. trifallax, P. tetraurelia,* and *T. thermophila,* have macronuclear genomes ranging from 50 to 103 Mb (Aury et al., 2006; Eisen et al., 2006; Swart et al., 2013). However, our estimate for *Loxodes* is not unfeasible for a ciliate, as the estimated DNA content of the *Blepharisma americanum* MAC is 42.6 Gb (Wancura et al., 2018). During the somatic macronuclear development from germline micronuclei, differential chromosome/gene replication and whole genome scale amplification may both occur, which usually results in high ploidy levels and larger amount of DNA in the somatic macronuclei (Prescott, 1994; Raikov, 1982). For instance, the ratio between the DNA content of macronuclei to micronuclei in *Bursaria truncatella* and *Spirostomum ambiguum* is approximately 5,240 and 13,150, respectively (Ovchinnikova et al., 1965; Ruthmann, 1964).

Both *H. papilio* and *Loxodes* display variation in nuclear number and genome content estimates (**Fig 4**; **Table 2**). This variation could result from the staining and imaging process, as cells do not always fix in the same orientation on the microscope slide, as well as sometimes substantial differences in nuclear volume among cells. Also, the variability could be influenced by the cell's life cycle stage, at the time when it was captured for the experiment. *Loxodes* micronuclei are generally diploid (e.g. Raikov, 1985; Parfrey et al, 2008), and thus we expect that cell cycle differences among samples will yield DNA content variability on the order of 2n to 4n.

Macronuclear DNA content may also vary substantially throughout Loxodes, and all ciliate, life cycles. Ploidy in adult *Loxodes* MACs has been observed to range from 4.5n-10n in some cases (Raikov, 1985). In some cases, encysted ciliates may decrease their DNA content through macronuclear extrusion (Akematsu and Matsuoka, 2008; Gutiérrez et al., 1998). Cyclical

endopolyploidzation and other examples of genome dynamics are widespread among eukaryotes (Parfrey and Katz, 2010b), and may contribute to the broad range of DNA content estimates in both *Loxodes* and *H. papilio*.

We also observe differences in DNA content between the macronuclei within an individual *Loxodes* cell, which concurs with Raikov's observations that young macronuclei tend to have less DNA than mature macronuclei, evident by less intense staining and smaller nuclear size (Raikov, 1985). Since the macronuclei in *Loxodes* are not capable of dividing, in every vegetative division, the daughter cell receives half of all macronuclei while the other half are generated anew from the germline micronuclei. Therefore, in *Loxodes*, the two macronuclei have gone through different numbers of vegetative divisions, which, in other words, shows the varied 'age' in the two somatic macronuclei (Raikov, 1985). As suggested in Bobyleva et al. (1980), mature macronuclei might undergo partial DNA amplification resulting in an increase in DNA content. The measured differences in *Loxodes* cells are supported by fluorescent images, in which we observe that one macronucleus in each cell is substantially smaller, dimmer, or has a less-developed nucleolus than the other. These data are a step towards validating the hypothesis that nuclear age differences cause differences in DNA content among macronuclei in Karyorelictea.

Synthesis

The newly developed and adapted protocols for uncultivable testate amoebae and ciliates, specifically, for *Hyalosphenia* spp. and *Loxodes* sp., successfully revealed the nuclear structure of the target lineages. Furthermore, we provide approximations of genome sizes using DAPI with three other model organisms. The protocols present in this work can be used for staining and estimating DNA content in uncultivable protists with modifications, which provides a useful

way to advance our knowledge in nuclear properties of diverse microbial eukaryotes, especially for those with few genomic/molecular data.

Acknowledgements

This study was supported by grants from the United States National Science Foundation (grant number OCE-1924570, DEB-1651908, DEB-1541511) and the United States National Institute of Health (grant number R15HG010409) to LAK. We are grateful to Judith Wopereis for training and help at the confocal microscope and to Dr. Joan Bernhard from Woods Hole Oceanographic Institution for her advice on fixation buffers. KM was funded by a McKinley Fellowship through the Achieving Excellence in Math Engineering and Science (AEMES) program. We thank members of the Katzlab for helpful comments on earlier versions of the manuscript.

References

- Akematsu, T., Matsuoka, T., 2008. Chromatin extrusion in resting encystment of Colpoda cucullus: A possible involvement of apoptosis-like nuclear death. Cell biology international 32, 31-38.
- Arnaiz, O., Mathy, N., Baudry, C., Malinsky, S., Aury, J.M., Wilkes, C.D., Garnier, O., Labadie, K., Lauderdale, B.E., Le Mouel, A., Marmignon, A., Nowacki, M., Poulain, J., Prajer, M., Wincker, P., Meyer, E., Duharcourt, S., Duret, L., Betermier, M., Sperling, L., 2012. The *Paramecium* germline genome provides a niche for intragenic parasitic DNA: evolutionary dynamics of internal eliminated sequences. Plos Genetics 8.
- Aury, J.M., Jaillon, O., Duret, L., Noel, B., Jubin, C., Porcel, B.M., Segurens, B., Daubin, V., Anthouard, V., Aiach, N., Arnaiz, O., Billaut, A., Beisson, J., Blanc, I., Bouhouche, K., Camara, F., Duharcourt, S., Guigo, R., Gogendeau, D., Katinka, M., Keller, A.M., Kissmehl, R., Klotz, C., Koll, F., Le Mouel, A., Lepere, G., Malinsky, S., Nowacki, M., Nowak, J.K., Plattner, H., Poulain, J., Ruiz, F., Serrano, V., Zagulski, M., Dessen, P., Betermier, M., Weissenbach, J., Scarpelli, C., Schachter, V., Sperling, L., Meyer, E., Cohen, J., Wincker, P., 2006. Global trends of whole-genome duplications revealed by the ciliate *Paramecium tetraurelia*. Nature 444, 171-178.
- Bellec, L., Maurer-Alcala, X.X., Katz, L.A., 2014. Characterization of the life cycle and heteromeric nature of the macronucleus of the ciliate *Chilodonella uncinata* using fluorescence microscopy. J. Euk. Micro. 61, 313–316.
- Bloomfield, G., 2016. Atypical ploidy cycles, Spo11, and the evolution of meiosis. Seminars in Cell & Developmental Biology 54, 158-164.
- Bobyleva, N., Kudrjavtsev, B., Raikov, I., 1980. Changes of the DNA content of differentiating and adult macronuclei of the ciliate *Loxodes magnus* (Karyorelictida). J. Cell Sci. 44, 375-394.
- Burdikova, Z., Capek, M., Ostasov, P., Machac, J., Pelc, R., Mitchell, E.A., Kubinova, L., 2010. Testate amoebae examined by confocal and two-photon microscopy: implications for taxonomy and ecophysiology. Microsc Microanal 16, 735-746.
- Button, D.K., Robertson, B.R., 2001. Determination of DNA content of aquatic bacteria by flow cytometry. Applied and Environmental Microbiology 67, 1636-1645.
- Byers, T.J., 1986. Molecular biology of DNA in *Acanthamoeba*, Amoeba, *Entamoeba*, and *Naegleria*. Int Rev Cytol 99, 311-341.
- Cavallini, F., 1926. The asexual cycle of development in *Arcella vulgaris*. Journal of Experimental Zoology 43, 245-255.
- Chávez-Munguía, B., Tsutsumi, V., Martínez-Palomo, A., 2006. *Entamoeba histolytica*: ultrastructure of the chromosomes and the mitotic spindle. Exp. Parasitol. 114, 235-239.
- Chen, X., Bracht, J.R., Goldman, A.D., Dolzhenko, E., Clay, D.M., Swart, E.C., Perlman, D.H., Doak, T.G., Stuart, A., Amemiya, C.T., Sebra, R.P., Landweber, L.F., 2014. The architecture of a scrambled genome reveals massive levels of genomic rearrangement during development. Cell 158, 1187-1198.
- Cousin, A., Heel, K., Cowling, W.A., Nelson, M.N., 2009. An efficient high-throughput flow cytometric method for estimating DNA ploidy level in plants. Cytometry Part A 75A, 1015-1019.
- Dumack, K., Gorzen, D., Gonzalez-Miguens, R., Siemensma, F., Lahr, D.J.G., Lara, E., Bonkowski, M., 2020. Molecular investigation of *Phryganella acropodia* Hertwig et Lesser, 1874 (Arcellinida, Amoebozoa). Eur J Protistol 75, 125707.
- Eisen, J.A., Coyne, R.S., Wu, M., Wu, D., Thiagarajan, M., Wortman, J.R., Badger, J.H., Ren, Q., Amedeo, P., Jones, K.M., Tallon, L.J., Delcher, A.L., Salzberg, S.L., Silva, J.C., Haas, B.J., Majoros, W.H., Farzad, M., Carlton, J.M., Smith, R.K., Garg, J., Pearlman, R.E., Karrer, K.M., Sun, L., Manning, G., Elde, N.C., Turkewitz, A.P., Asai, D.J., Wilkes, D.E., Wang, Y.,

- Cai, H., Collins, K., Stewart, B.A., Lee, S.R., Wilamowska, K., Weinberg, Z., Ruzzo, W.L., Wloga, D., Gaertig, J., Frankel, J., Tsao, C.C., Gorovsky, M.A., Keeling, P.J., Waller, R.F., Patron, N.J., Cherry, J.M., Stover, N.A., Krieger, C.J., Del Toro, C., Ryder, H.F., Williamson, S.C., Barbeau, R.A., Hamilton, E.P., Orias, E., 2006. Macronuclear genome sequence of the ciliate *Tetrahymena thermophila*, a model eukaryote. PLoS Biol 4, e286.
- Finlay, B., Berninger, U.-G., 1984. Coexistence of congeneric ciliates (Karyorelictida: *Loxodes*) in relation to food resources in two freshwater lakes. The Journal of Animal Ecology 53, 929-943.
- Friz, C.T., 1968. The biochemical composition of the free-living Amoebae *Chaos chaos*, *Amoeba dubia* and *Amoeba proteus*. Comparative Biochemical Physiology 26, 81-90.
- Goodkov, A.V., Berdieva, M.A., Podlipaeva, Y.I., Demin, S.Y., 2020. The Chromatin Extrusion Phenomenon in *Amoeba proteus* Cell Cycle. Journal of Eukaryotic Microbiology 67, 203-208.
- Grattepanche, J.D., Walker, L.M., Ott, B.M., Pinto, D.L.P., Delwiche, C.F., Lane, C.E., Katz, L.A., 2018. Microbial Diversity in the Eukaryotic SAR Clade: Illuminating the Darkness Between Morphology and Molecular Data. BioEssays 40.
- Griffin, J., 1972. Movement, fine structure, and fusion of pseudopods of an enclosed amoeba, *Difflugiella* sp. J. Cell Sci. 10, 563-583.
- Gutiérrez, J.C., Martin-González, A., Callejas, S., 1998. Nuclear changes, macronuclear chromatin reorganization and DNA modifications during ciliate encystment. European Journal of Protistology 34, 97-103.
- Hamilton, E.P., Kapusta, A., Huvos, P.E., Bidwell, S.L., Zafar, N., Tang, H.B., Hadjithomas, M., Krishnakumar, V., Badger, J.H., Caler, E.V., Russ, C., Zeng, Q.D., Fan, L., Levin, J.Z., Shea, T., Young, S.K., Hegarty, R., Daza, R., Gujja, S., Wortman, J.R., Birren, B.W., Nusbaum, C., Thomas, J., Carey, C.M., Pritham, E.J., Feschotte, C., Noto, T., Mochizuki, K., Papazyan, R., Taverna, S.D., Dear, P.H., Cassidy-Hanley, D.M., Xiong, J., Miao, W., Orias, E., Coyne, R.S., 2016. Structure of the germline genome of *Tetrahymena thermophila* and relationship to the massively rearranged somatic genome. Elife 5.
- Huang, J., Katz, L.A., 2014. Nanochromosome Copy Number Does not Correlate with RNA Levels Though Patterns are Conserved between Strains of the Ciliate Morphospecies *Chilodonella uncinata*. Protist 165, 445-451.
- Lahr, D.J.G., Kosakyan, A., Lara, E., Mitchell, E.A.D., Morais, L., Porfirio-Sousa, A.L., Ribeiro, G.M., Tice, A.K., Panek, T., Kang, S., Brown, M.W., 2019. Phylogenomics and morphological reconstruction of arcellinida testate amoebae highlight diversity of microbial eukaryotes in the neoproterozoic. Curr Biol 29, 991-1001 e1003.
- Loureiro, J., Rodriguez, E., Doležel, J., Santos, C., 2006. Comparison of four nuclear isolation buffers for plant DNA flow cytometry. Ann. Bot. 98, 679-689.
- Maurer-Alcalá, X.X., Katz, L.A., 2016. Nuclear architecture and patterns of molecular evolution are correlated in the ciliate *Chilodonella uncinata*. Genome Biology and Evolution, evw099.
- Mazei, Y., Warren, A., 2014. A survey of the testate amoeba genus *Difflugia* Leclerc, 1815 based on specimens in the E. Penard and CG Ogden collections of the Natural History Museum, London. Part 2: Species with shells that are pyriform or elongate. Protistology 8, 133–171.
- McGrath, C.L., Katz, L.A., 2004. Genome diversity in microbial eukaryotes. Trends Ecol. Evol. 19. 32-38.
- Mieczan, T., 2009. Ecology of testate amoebae (Protists) in *Sphagnum* peatlands of eastern Poland: vertical micro-distribution and species assemblages in relation to environmental parameters. Annales de limnologie-International journal of limnology 45, 41-49.
- Mignot, J.-P., Raikov, I.B., 1992. Evidence for meiosis in the testate amoeba *Arcella*. Journal of Eurkaryotic Microbiology 39, 287-289.

- Mitchell, E.A.D., Charman, D.J., Warner, B.G., 2008. Testate amoebae analysis in ecological and paleoecological studies of wetlands: past, present and future. Biodivers. Conserv. 17, 2115-2137.
- Mitchell, E.A.D., Meisterfeld, R., 2005. Taxonomic confusion blurs the debate on cosmopolitanism versus local endemism of free-living protists. Protist 156, 263-267.
- Montanaro, J., Gruber, D., Leisch, N., 2016. Improved ultrastructure of marine invertebrates using non-toxic buffers. PeerJ 4, e1860.
- Mukherjee, C., Majumder, S., Lohia, A., 2009. Inter-cellular variation in DNA content of *Entamoeba histolytica* originates from temporal and spatial uncoupling of cytokinesis from the nuclear cycle. PLoS Negl Trop Dis 3, e409.
- Nikolaev, S.I., Mitchell, E.A.D., Petrov, N.B., Berney, C., Fahrni, J., Pawlowski, J., 2005. The testate lobose amoebae (order Arcellinida Kent, 1880) finally find their home within Amoebozoa. Protist 156, 191-202.
- Noirot, M., Barre, P., Louarn, J., Duperray, C., Hamon, S., 2002. Consequences of stoichiometric error on nuclear DNA content evaluation in *Coffea liberica* var. *dewevrei* using DAPI and propidium iodide. Ann. Bot. 89, 385-389.
- Ovchinnikova, L., Cheissin, E., Selivanova, G., 1965. Photometric study of the DNA content in the nuclei of *Spirostomum ambiguum* (Ciliata, Heterotricha).
- Palazzo, A.F., Gregory, T.R., 2014. The case for junk DNA. PLoS Genet 10, e1004351.
- Parfrey, L.W., Katz, L.A., 2010a. Dynamic genomes of eukaryotes and the maintenance of genomic integrity. Microbe 5, 156-164.
- Parfrey, L.W., Katz, L.A., 2010b. Genome dynamics are influenced by food source in *Allogromia laticollaris* strain CSH (Foraminifera). Genome Biol Evol 2, 678-685.
- Parfrey, L.W., Lahr, D.J.G., Katz, L.A., 2008. The dynamic nature of eukaryotic genomes. Molecular Biology and Evolution 25, 787-794.
- Piovesan, A., Pelleri, M.C., Antonaros, F., Strippoli, P., Caracausi, M., Vitale, L., 2019. On the length, weight and GC content of the human genome. Eur J Hum Genet 27, 583-583.
- Prescott, D.M., 1994. The DNA of ciliated protozoa. Microbiological Reviews 58, 233-267.
- Raikov, I.B., 1982. The Protozoan Nucleus: Morphology and Evolution. Springer-Verlag, Wien.
- Raikov, I.B., 1985. Primitive never-dividing macronuclei of some lower ciliates. International review of cytology 95, 267-325.
- Ricroch, A., Brown, S.C., 1997. DNA base composition of Allium genomes with different chromosome numbers. Gene 205, 255-260.
- Ron, A., Urieli, S., 1977. Qualitative and quantitative studies on DNA and RNA synthesis in *Loxodes striatus* nuclei. J Protozool 24, 150-154.
- Ruthmann, A., 1964. Autoradiographische und mikrophotometrische Untersuchungen zur DNS-Synthese im Makronucleus von *Bursaria truncatella*. . Arch. Protistenk. 107, 117-130.
- Sime-Ngando, T., Hartmann, H.J., Groliere, C.A., 1990. Rapid quantification of planktonic ciliates: comparison of improved live counting with other methods. Applied and Environmental Microbiology 56, 2234-2242.
- Suda, J., Trávníček, P., 2006. Reliable DNA ploidy determination in dehydrated tissues of vascular plants by DAPI flow cytometry—new prospects for plant research. Cytometry Part A 69, 273-280.
- Sun, H.Y., Noe, J., Barber, J., Coyne, R.S., Cassidy-Hanley, D., Clark, T.G., Findly, R.C., Dickerson, H.W., 2009. Endosymbiotic Bacteria in the Parasitic Ciliate *Ichthyophthirius multifiliis*. Applied and Environmental Microbiology 75, 7445-7452.
- Swart, E.C., Bracht, J.R., Magrini, V., Minx, P., Chen, X., Zhou, Y., Khurana, J.S., Goldman, A.D., Nowacki, M., Schotanus, K., Jung, S., Fulton, R.S., Ly, A., McGrath, S., Haub, K., Wiggins, J.L., Storton, D., Matese, J.C., Parsons, L., Chang, W.J., Bowen, M.S., Stover, N.A., Jones, T.A., Eddy, S.R., Herrick, G.A., Doak, T.G., Wilson, R.K., Mardis, E.R.,

- Landweber, L.F., 2013. The *Oxytricha trifallax* Macronuclear Genome: A Complex Eukaryotic Genome with 16,000 Tiny Chromosomes. PLoS Biology 11.
- Swindles, G.T., Green, S.M., Brown, L., Holden, J., Raby, C.L., Turner, T.E., Smart, R., Peacock, M., Baird, A.J., 2016. Evaluating the use of dominant microbial consumers (testate amoebae) as indicators of blanket peatland restoration. Ecological Indicators 69, 318-330.
- Volkova, E., Smirnov, A., 2016. Regeneration of test in testate amoebae of the genus *Arcella* (Tubulinea, Arcellinida). European Journal of Protistology 55, 128-140.
- Wancura, M.M., Yan, Y., Katz, L.A., Maurer-Alcalá, X.X., 2018. Nuclear features of the heterotrich ciliate *Blepharisma americanum*: genomic amplification, life cycle, and nuclear inclusion. J Eukaryot Microbiol 65, 4-11.
- Wang, D., Gao, F., 2019. Comprehensive Analysis of Replication Origins in *Saccharomyces cerevisiae* Genomes. Front Microbiol 10.
- Weber, A.A., Pawlowski, J., 2013. Can abundance of protists be inferred from sequence data: a case study of Foraminifera. PloS one 8, e56739.
- Weiner, A.K.M., Yan, Y., Ceron Romero, M., Katz, L.A., 2020. Phylogenomics of the eukaryotic epigenetic toolkit reveals punctate retention of genes across lineages and functional categories. Gen Biol Evol evaa198.
- Wheeler, R.J., Gull, K., Gluenz, E., 2012. Detailed interrogation of trypanosome cell biology via differential organelle staining and automated image analysis. Bmc Biology 10.
- Yan, Y., Maurer-Alcala, X.X., Knight, R., Kosakovsky Pond, S.L., Katz, L.A., 2019. Single-Cell Transcriptomics Reveal a Correlation between Genome Architecture and Gene Family Evolution in Ciliates. mBio 10.
- Yan, Y., Rogers, A.J., Gao, F., Katz, L.A., 2017. Unusual features of non-dividing somatic macronuclei in the ciliate class Karyorelictea. Eur J Protistol 61, 399-408.

Figure Legends:

Figure 1. Flowchart showing the main methodological steps used in DAPI staining of both, *Hyalosphenia* and *Loxodes*. The drawings in the center illustrate the sampling sites for the uncultivable focal taxa *Hyalosphenia* and *Loxodes*, respectively. The two protocols for Arcellinida and ciliates mainly differ in the fixation step (Step 2, PHEM buffer for Arcellinida vs. 20% PFA for *Loxodes*).

Figure 2: Exemplar cells of *Loxodes* sp. (A, B), *Hyalosphenia elegans* (C, D) and *H. papilio* (E, F) successfully stained with DAPI and the corresponding DIC images. Red arrows show the location of nuclei in the DIC images. MIC: germline micronuclei; MAC: somatic macronuclei. Scales bars: 50 μm.

Figure 4: Estimates of DNA content from study organisms, *Loxodes* sp. and *Hyalosphenia papilio*, plus control organisms (*Homo sapiens, Allium cepa, Saccharomyces cerevisiae*). (A) Scatter plot showing a linear relationship between total nuclear fluorescence intensity (F) and nuclear volume (in μm³). (B) boxplot showing estimates of DNA content (bp) for all organisms (see Table 2).

Figure 3: Examples of DAPI and corresponding DIC images of cells from model organisms used for establishing standard curves. (A, B) *Homo sapiens*; (C, D) *Allium cepa*; (E, F) *Saccharomyces cerevisiae*. DAPI staining carried out following the *Hyalosphenia* protocol. Scale bars = 25 μ m (A, B, E, F), 200 μ m (C, D).

Table 1. Summary of observations and measurements conducted on the cells of each of the focal organisms in this study (*Loxodes*, *Hyalosphenia papilio* and *Hyalosphenia elegans*) as well as the standards (*Homo sapiens*, *Allium cepa* and *Saccharomyces cerevisiae*). Atypical cells are those with more than two macronuclei for *Loxodes*, and more than one nucleus for *H. papilio*. Average nuclear diameter is calculated from cell volume that measured in NIS-Elements Advanced Research software. MAC = somatic macronucleus, MIC = germline micronucleus.

Organism	# Cells measured	# Atypical cells				
Loxodes sp. MAC	29	59	1	6.6		
<i>Loxodes</i> sp. MIC	29	67	5	3.5		
Hyalosphenia papilio	25	35	5	18.3 (uninucleate) 11.4 (multinucleate)		
Hyalosphenia elegans	3	3	0	10.7		
Saccharomyce s cerevisiae	63	63	0	1.8		
Homo sapiens	43	43	0	7.8		
Allium cepa	19	19	0	11.1		

Table 2: Average fluorescence intensity (in thousands of fluorescence units), average genome size estimates with standard deviation, and range of estimated DNA content observed from standards (*Saccharomyces cerevisiae*, *Homo sapiens* and *Allium cepa*) and the focal microbes used in this study. DNA contents of *Loxodes* sp. and *Hyalosphenia papilio* were estimated based on the average ratio of fluorescence to DNA content across the three standards. MAC = somatic macronucleus, MIC = germline micronucleus.

Organism	Avg. fluor. (K)	Average DNA content (Mb) ± SD	Min. DNA content (Mb) – Max. DNA content (Mb)
Loxodes sp. MAC	$2,120 \pm 1,037$	$3,500 \pm 1,732$	705 – 7,325
Loxodes sp. MIC	841 ± 555	$\textbf{1,400} \pm \textbf{927}$	182 – 3,782
Uninucleate Hyalosphenia. papilio	$15,032 \pm 10,634$	$20,\!900 \pm 17,\!759$	4,407 – 61,021
Multinucleate <i>Hyalosphenia.</i> papilio	12,538 ± 4,915	11,200 ± 8,209	1,872 – 32,727
Saccharomyces cerevisiae	98 ± 39	13 ± 5	6 – 25
Homo sapiens	3,139 ± 1,031	$3,300 \pm 1,084$	953 – 5,216
Allium cepa	4,145 ± 1,249	$15,876 \pm 4,783$	8,376 – 24,067

Figure 1: Flowchart showing the main methodological steps used in DAPI staining of both, *Hyalosphenia* and *Loxodes*. The drawings in the center illustrate the sampling sites for the uncultivable focal taxa *Hyalosphenia* and *Loxodes*, respectively. The two protocols for *Hyalosphenia* and *Loxodes* mainly differ in the fixation step (Step 2, PHEM buffer for *Hyalosphenia* vs. 20% PFA for *Loxodes*).

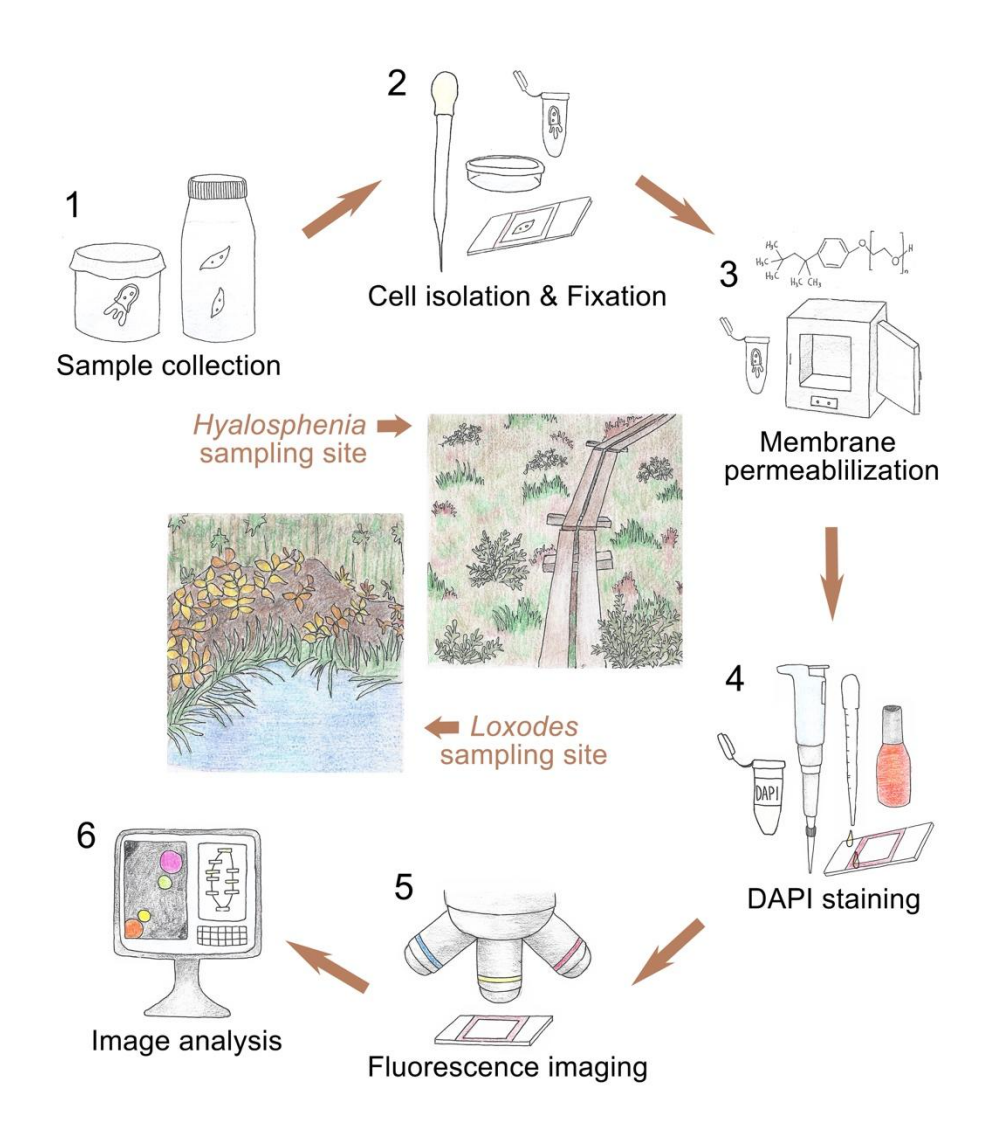


Figure 2: Exemplar cells of *Loxodes* (A, B), *Hyalosphenia elegans* (C, D) and *Hyalosphenia papilio* (E, F) successfully stained with DAPI and the corresponding DIC images. Red arrows show the location of nuclei in the DIC images. MIC: germline micronuclei; MAC: somatic macronuclei. Scales bars: 50 μm.

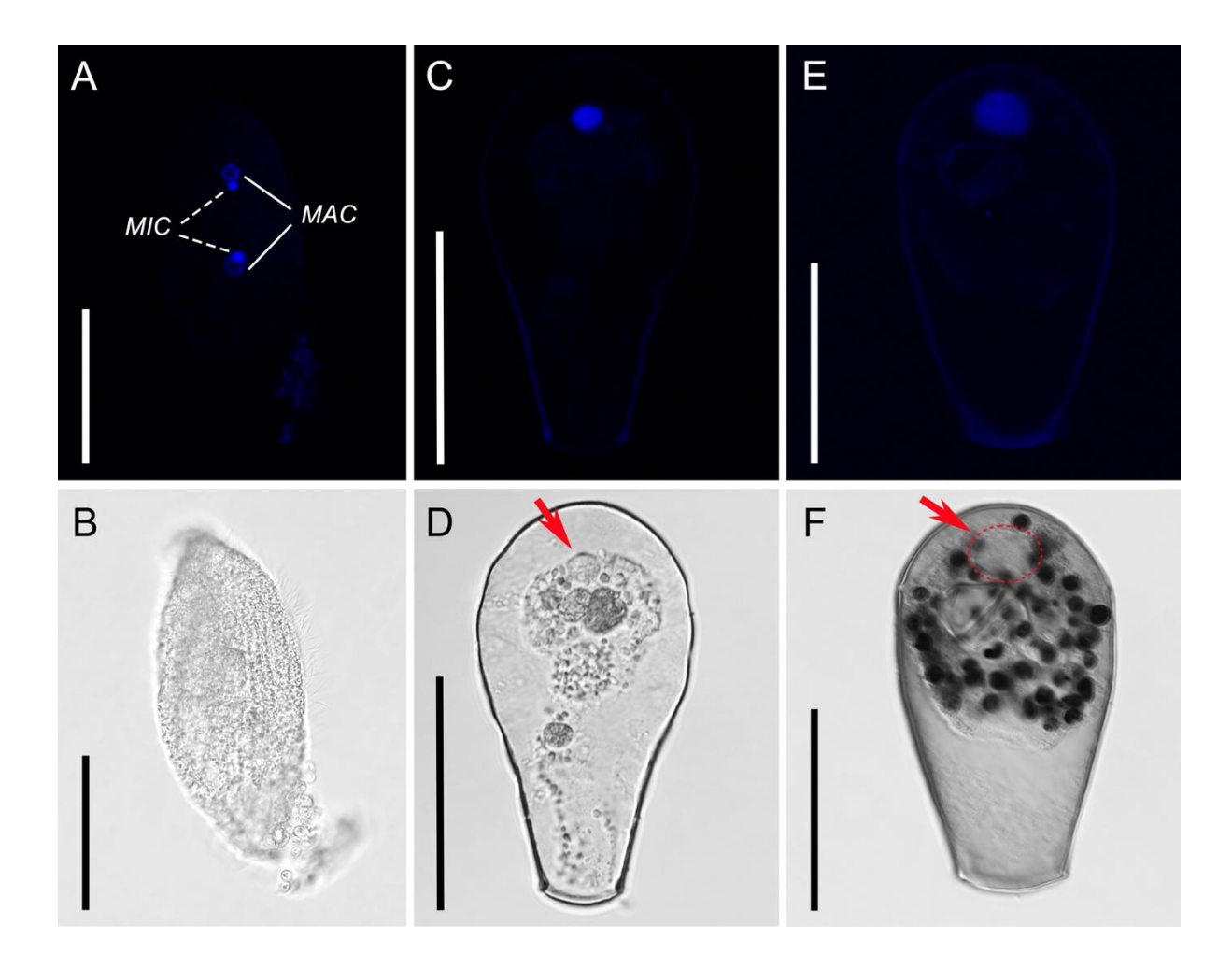


Figure 3: Examples of DAPI and corresponding DIC images of cells from model organisms used for establishing standard curves. (A, B) *Homo sapiens*; (C, D) *Allium cepa*; (E, F) *Saccharomyces cerevisiae*. DAPI staining carried out following the PHEM protocol for *Hyalosphenia*. Scale bars = 25 μ m (A, B, E, F), 200 μ m (C, D).

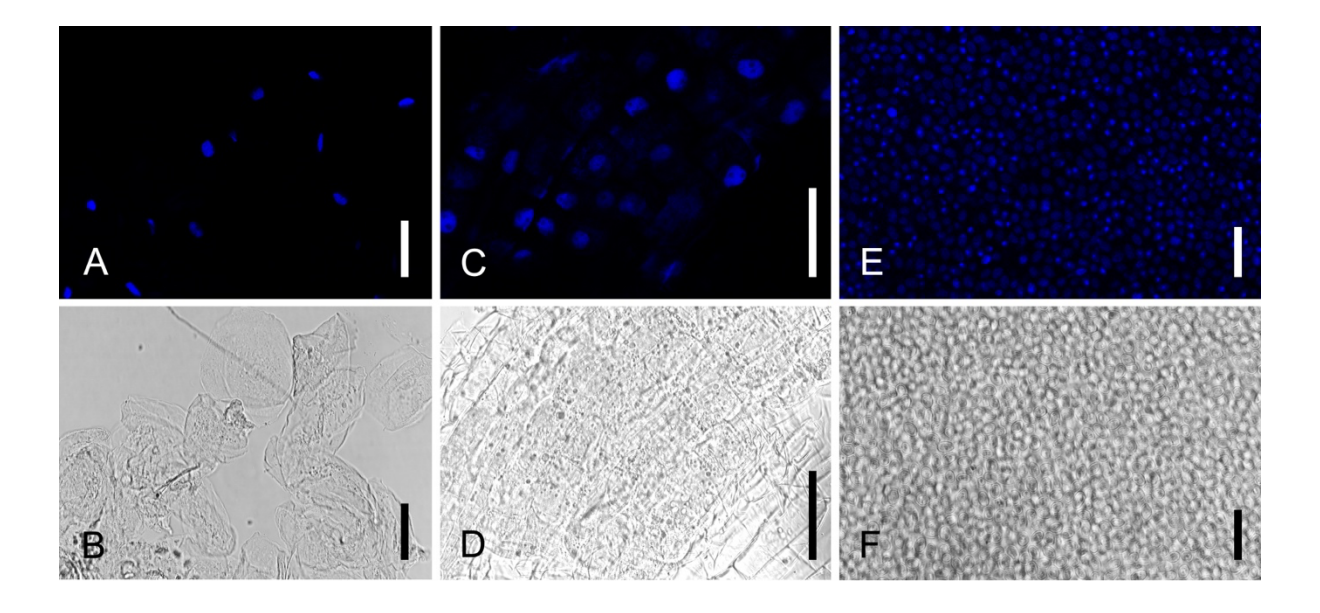
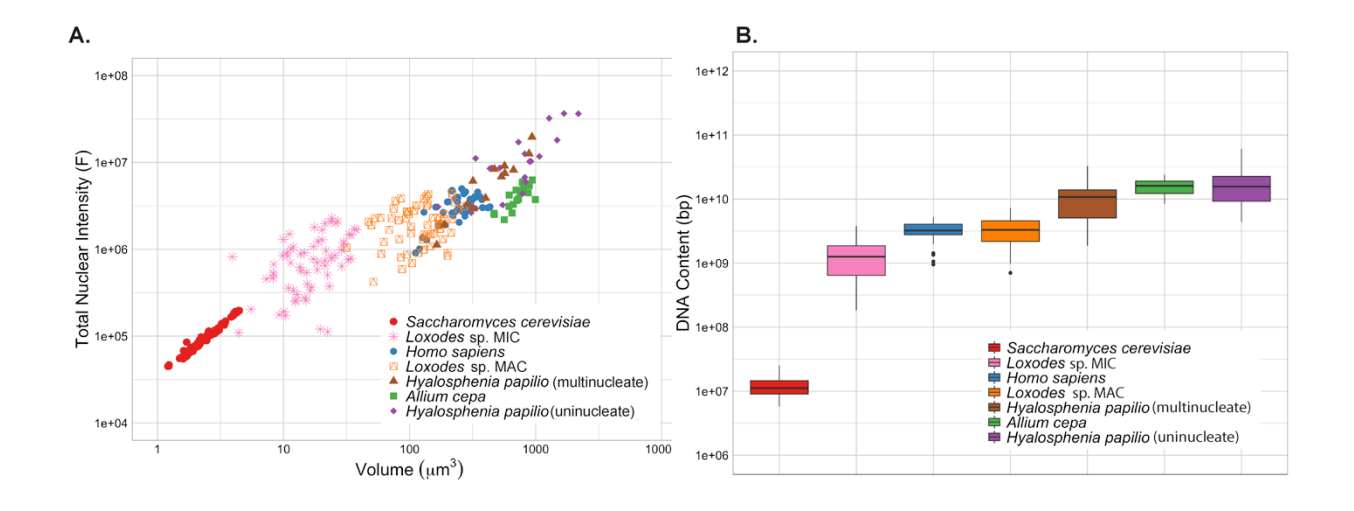


Figure 4: Estimates of DNA content from *Loxodes*, *Hyalosphenia papilio* and control organisms (*Homo sapiens, Allium cepa, Saccharomyces cerevisiae*). (A) Scatter plot showing a linear relationship between total nuclear fluorescence intensity (F) and nuclear volume (in μm³). (B) boxplot showing estimates of DNA content (bp) for all organisms (see Table 2).



Supplementary figure and tables

Figure S1: Cells of *Loxodes* (A, B) and *H. papilio* (C, D) with multiple nuclei as seen in DAPI and corresponding DIC images. Scales bars: 50 μm.

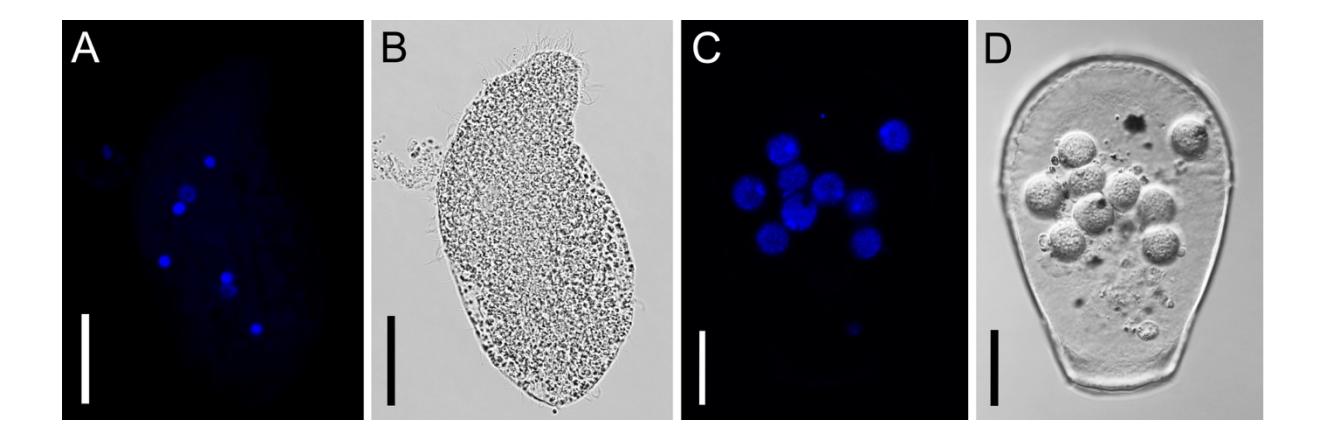


Figure S2: Scatterplot comparing the total nuclear fluorescence intensity (F) and nuclear volume (in μ m³) of focal organisms and standard cells stained according to both the PHEM protocol for *Hyalosphenia* and the PFA protocol for *Loxodes*. Circular grey points denote *S. cerevisiae* cells stained according to the PHEM protocol for *Hyalosphenia* that were densely arranged on slides and excluded from final analyses. Square grey points denote *A. cepa* cells stained according to the PFA protocol for *Loxodes* that were affected by slide debris and excluded from final analyses.

Table S1: Total nuclear intensity of the standards *Saccharomyces cerevisiae*, *Homo sapiens*, and *Allium cepa* as measured after application of the two nuclear staining protocols for *Hyalosphenia* and *Loxodes*. Avg., average; Min., minimum; Max., maximum.

Standards	Protocol	Protocol Avg. Fluorescence (F)		Max. Fluorescence (F)
Saccharomyces	Arcellinida	35,841	13,549	69,987
cerevisiae	Ciliate	97,863	44,933	196,380
Homo sapiens	Arcellinida	4,145,464	2,187,018	6,283,847
	Ciliate	3,009,364	853,538	5,935,190
Allium cepa	Arcellinida	3,139,734	906,655	4,962,429
	Ciliate	1,974,989	694,146	4,998,302

Table S2: Raw measurements of nuclear volume and fluorescence intensity (F) for each cell investigated in this study. Fluorescence integrated over volume and volumes for cells were directly calculated using Nikon NIS-Elements AR software. Bottom row contains averages for each column.

	Saccharomyces cerevisiae Allium cepa		Homo sapiens		Loxodes sp. macronucleus		Loxodes sp. micronucleus		Hyalosphenia papilio uninucleate		Hyalosphenia papilio multinucleated		
μm ³	F	μm³	F	µm³	F	μm³	F	µm³	F	μm³	F	µm³	F
4.5	2.0E+05	5.6E+02	2.2E+06	1.7E+02	1.9E+06	1.0E+02	6.9E+05	15.1	2.6E+05	5.5E+02	3.2E+06	9.4E+02	2.0E+07
4.0	1.8E+05	9.9E+02	3.7E+06	1.8E+02	1.9E+06	8.7E+01	5.9E+05	14.8	2.7E+05	4.5E+02	8.6E+06	4.7E+02	8.4E+06
1.8	6.3E+04	6.5E+02	2.6E+06	2.8E+02	2.7E+06	8.2E+01	2.1E+06	10.3	1.7E+05	8.3E+02	6.0E+06	3.2E+02	6.1E+06
2.5	9.0E+04	7.1E+02	3.6E+06	3.0E+02	2.9E+06	9.9E+01	2.5E+06	13.5	6.2E+05	3.3E+02	1.1E+07	1.6E+02	1.1E+06
1.9	6.9E+04	8.9E+02	5.4E+06	2.5E+02	2.0E+06	7.5E+01	2.9E+06	17.3	7.7E+05	7.9E+02	4.4E+06	4.0E+02	3.9E+06
2.6	1.0E+05	7.6E+02	4.5E+06	2.0E+02	3.5E+06	5.0E+01	1.9E+06	25.9	2.0E+06	8.2E+02	6.7E+06	2.9E+02	3.3E+06
3.3	1.4E+05	6.6E+02	3.3E+06	1.6E+02	3.1E+06	8.6E+01	3.8E+06	8.3	4.6E+05	3.1E+02	2.6E+06	5.7E+02	9.1E+06
2.0	7.2E+04	7.8E+02	4.7E+06	4.3E+02	3.1E+06	7.7E+01	3.6E+06	17.6	1.8E+06	8.2E+02	1.3E+07	1.9E+02	1.9E+06
2.2	9.8E+04	8.7E+02	4.5E+06	3.8E+02	3.0E+06	1.8E+02	1.3E+06	8.3	5.3E+05	3.4E+02	2.9E+06	3.2E+02	2.9E+06
2.1	8.5E+04	7.8E+02	5.9E+06	3.0E+02	3.1E+06	1.7E+02	2.0E+06	12.4	2.5E+05	1.7E+02	3.1E+06	3.2E+02	2.9E+06
2.3	9.1E+04	7.3E+02	3.8E+06	2.8E+02	4.6E+06	1.3E+02	1.5E+06	9.2	1.8E+05	1.1E+03	1.2E+07	8.9E+02	1.3E+07
2.2	8.6E+04	4.7E+02	2.5E+06	1.1E+02	9.1E+05	1.5E+02	1.5E+06	30.0	1.2E+06	8.9E+02	1.0E+07	5.7E+02	7.5E+06
1.2	4.7E+04	4.7E+02	2.6E+06	2.8E+02	2.8E+06	5.2E+01	4.2E+05	15.3	5.4E+05	1.3E+03	3.2E+07	6.7E+02	8.2E+06
2.2	9.0E+04	9.4E+02	6.3E+06	1.2E+02	1.0E+06	2.3E+02	3.5E+06	18.6	7.0E+05	2.2E+03	3.6E+07	5.3E+02	6.8E+06
3.0	1.2E+05	7.0E+02	4.8E+06	2.5E+02	3.0E+06	1.0E+02	1.8E+06	10.9	3.6E+05	1.5E+03	1.8E+07		
1.5	5.7E+04	8.0E+02	6.0E+06	2.7E+02	2.4E+06	1.1E+02	3.2E+06	8.3	5.1E+05	1.7E+03	3.7E+07		
1.9	6.8E+04	6.2E+02	4.2E+06	2.3E+02	2.8E+06	6.9E+01	1.7E+06	13.6	8.8E+05	4.3E+02	8.5E+06		
2.1	8.0E+04	8.0E+02	5.1E+06	3.0E+02	3.8E+06	9.5E+01	2.7E+06	11.4	7.0E+05	5.2E+02	8.6E+06		
2.5	1.0E+05	6.1E+02	3.1E+06	2.6E+02	2.8E+06	1.3E+02	3.8E+06	20.2	1.3E+06	7.3E+02	1.7E+07		
3.1	1.2E+05			3.7E+02	3.7E+06	7.2E+01	2.3E+06	20.3	1.7E+06	9.2E+02	1.0E+07		
1.9	7.6E+04			3.3E+02	4.0E+06	1.4E+02	4.3E+06	24.1	2.3E+06				
1.6	6.8E+04			4.2E+02	3.0E+06	1.0E+02	1.5E+06	26.9	2.1E+06				

4.0 1.2 4 1.2 4 3.5 2.5 2.8 1.7 2.4 9 2.8	8.8E+04 1.7E+05 4.5E+04 4.5E+04 1.5E+05 1.1E+05 1.2E+05	2.2E+02	2.4E+06		1.3E+06		4.5E+05		ĺ
1.2 4 1.2 4 3.5 2.5 2.8 1.7 5 2.4 9 2.8 2.8 2.8 2.8 2.8 2.8 2.8 2.8 2.8 2.8	4.5E+04 4.5E+04 1.5E+05 1.1E+05		2.4E+06	1 1 = +02					
1.2 4 3.5 2.5 2.8 1.7 2.4 9 2.8 2.8	4.5E+04 1.5E+05 1.1E+05 1.2E+05	$10 \text{ MH} \cdot 100$				5.5	2.0E+05		
3.5 2.5 2.8 1.7 4 2.4 9 2.8	1.5E+05 1.1E+05 1.2E+05		3.8E+06				5.6E+05		
2.5 2.8 1.7 2.4 2.8	1.1E+05 1.2E+05		3.2E+06			17.2	1.1E+06		
2.8 · · · · · · · · · · · · · · · · · · ·	1.2E+05		4.6E+06			14.6	9.1E+05		
1.7		2.2E+02	2.6E+06	1.9E+02	2.5E+06	3.9	8.2E+05		
2.4		3.6E+02	4.0E+06	6.0E+01	8.8E+05	12.5	2.6E+05		
2.8	5.8E+04	3.1E+02	3.6E+06	9.6E+01	8.7E+05	34.0	7.8E+05		
	9.2E+04	1.3E+02	1.4E+06	1.6E+02	1.5E+06	19.6	1.2E+05		
	1.1E+05	2.0E+02	3.5E+06	1.8E+02	2.0E+06	22.4	1.1E+05		
1.7	8.5E+04	2.3E+02	3.8E+06	1.4E+02	1.9E+06	4.4	1.1E+05		
2.1	8.3E+04	2.1E+02	4.7E+06	2.0E+02	9.1E+05	15.4	4.0E+05		
1.9	7.4E+04	2.7E+02	4.4E+06	2.0E+02	8.4E+05	12.8	3.0E+05		
3.2	1.4E+05	1.3E+02	2.7E+06	1.5E+02	1.1E+06	21.4	6.5E+05		
2.6	1.1E+05	2.7E+02	4.6E+06	1.2E+02	9.1E+05	28.9	9.8E+05		
2.5	1.1E+05	3.4E+02	4.0E+06	1.4E+02	1.4E+06	23.1	3.7E+05		
1.6	5.5E+04	1.8E+02	2.7E+06	1.3E+02	1.3E+06	10.1	1.9E+05		
2.0	7.4E+04	1.9E+02	1.9E+06	3.2E+01	1.0E+06	22.3	5.0E+05		
1.9	6.7E+04	2.4E+02	4.0E+06	5.9E+01	2.3E+06	32.6	7.6E+05		
3.0	1.1E+05	2.4E+02	3.5E+06	2.2E+02	4.4E+06	25.5	8.5E+05		
2.1	7.8E+04	2.2E+02	4.8E+06	2.2E+02	4.4E+06	24.0	7.9E+05		
2.1	7.9E+04	2.6E+02	5.0E+06	2.7E+02	3.1E+06	11.1	1.5E+06		
2.1	7.6E+04			1.7E+02	2.3E+06	9.9	1.3E+06		
4.2	1.8E+05			9.4E+01	2.3E+06	28.9	6.4E+05		
4.1	1.9E+05			9.6E+01	2.7E+06	23.9	7.9E+05		
2.7	1.0E+05			2.2E+02	2.2E+06	33.1	1.5E+06		
3.8	1.7E+05			2.1E+02	1.5E+06	37.9	1.7E+06		
2.9	1.1E+05			1.7E+02	1.7E+06	30.1	1.2E+06		
4.4	2.0E+05			1.3E+02	9.9E+05	10.8	8.4E+05		
2.1	7.6E+04			1.4E+02	3.1E+06	23.8	2.1E+06		
3.4	1.3E+05			1.4E+02	3.3E+06	34.5	1.5E+06		
1.7	6.6E+04			2.4E+02	2.9E+06	21.2	7.4E+05		
1.8	7.2E+04			6.3E+01	1.2E+06	12.0	3.4E+05		
2.5	8.9E+04			4.8E+01	2.1E+06	18.5	5.8E+05		
1.8	6.9E+04			5.3E+01	2.3E+06	18.8	1.2E+06		
1.6	5.7E+04			1.5E+02	2.3E+06	21.3	2.0E+06		
1.5	5.5E+04			8.5E+01	8.1E+05	36.4	1.7E+06		
2.2	8.2E+04					16.3	3.4E+05		
3.4	1.4E+05					11.5	1.0E+06		
1.7	6.1E+04					12.0	1.1E+06		
2.2	8.7E+04					9.9	8.4E+05		
3.4	1.4E+05 6.1E+04					11.5 12.0	1.0E+06 1.1E+06		

2.4	9.8E+04	7.3+E02	4.1E+06	2.5E+02	3.1E+06	1.3E+02	2.1E+06	18.0	8.4E+05	8.E+02	1.3E+07	4.7E+02	6.7E+06
								16.7	3.7E+05				
									9.6E+05				
								8.3	6.7E+05				
								10.6	9.1E+05				